Optimization and Comparison of Superconducting Generator Topologies for a 10 MW Wind Turbine Application

Dong Liu[1*], Henk Polinder[1], Asger B. Abrahamsen[2], Ewoud Stehouwer[3], Ben Hendriks[3], and Niklas Magnusson[4]

[1]Electrical Sustainable Energy Department, Delft University of Technology, Mekelweg 4, 2628 CD Delft, Netherlands. E-mail: d.liu-1@tudelft.nl, h.polinder@tudelft.nl

[2]DTU Wind Energy, Technical University of Denmark, Frederiksborgvej 399, 4000 Roskilde, Denmark. E-mail: asab@dtu.dk

[3]DNV-GL, Leiden, Netherlands. E-mail: ewoud.stehouwer@dnvgl.com, ben.hendriks@dnvgl.com

[4]SINTEF Energy Research, Trondheim, Norway. E-mail: niklas.magnusson@sintef.no

[*]Corresponding author. Electrical Sustainable Energy Department, Delft University of Technology, Mekelweg 4, 2628 CD Delft, Netherlands. E-mail: d.liu-1@tudelft.nl. Tel. no.: (+31)(0)152789849. Fax no.: (+31)(0)152782968

Abstract

A direct-drive superconducting generator (DDSCG) is proposed for 10 MW wind turbines in the INNWIND.EU project. To fit the generator into the "king-pin" conceptual nacelle design, the generator structure with inner stationary superconducting (SC) field winding and outer rotating copper armature winding is investigated in the first research phase. This paper presents a method using 2D finite element (FE) methods to minimize the active material cost of the "king-pin" fitted DDSCG by optimizing the geometrical variables. By implementing this method, three typical superconducting generator topologies are compared in terms of the active material cost and mass, the synchronous reactance and the phase resistance. The optimization method and the comparison results provide the DDSCG designers with a guideline for selecting a suitable machine topology.

1 Introduction

Single offshore wind turbines under consideration are approaching the 10 MW (or above) power level, since a larger turbine could reduce the cost of energy. With such a high power, conventional wind turbine generators encounter several significant problems [1], [2]. Direct-drive generators tend to be very large and heavy and geared generators have to use very big, complex and expensive gearboxes. A few future wind turbine generator systems have been proposed and developed to address these problems [3]. One of them is a direct-drive superconducting (SC) generator (DDSCG) which is able to considerably reduce the generator size and weight by boosting the torque density [4]-[6].

Superconductors carry high current densities practically without energy losses when cooled down below their critical current density. Although the implementation of both SC field and armature windings in an electrical machine, e.g. a wind turbine generator, may seem quite interesting and attractive [7], the application of superconductor wires has been extensively proposed for the field winding operated in a DC field environment [8] because the AC losses ([9], [10]) appearing in armature superconductor wires (exposed to AC magnetic fields and currents) are unacceptably high [11]. In the latter type, the armature winding is made of copper and hence, the superconductor wires experience only low losses due to magnetic field ripples and possibly by DC losses if operated close to their critical current. The cooling system therefore mainly has to deal with the heat in-leak from the surroundings and becomes much less complicated and expensive than a cooling system for a fully SC generator.

A novel wind turbine nacelle, which applies a stationary shaft "king-pin" architecture with the generator mounted in front of the hub, is proposed in the INNWIND.EU project [12] (see Fig. 1). A DDSCG with superconducting field winding and copper armature winding is being designed to fit this novel nacelle. A suitable option of the generator structure is thus inner stationary superconducting field winding with outer rotating copper armature winding [13]. Three typical superconducting machine topologies are proposed under this structure: non-magnetic core with iron armature yoke (T1), non-magnetic armature teeth with iron yokes (T2) and iron core (T3) [14]-[16].

A key performance indicator which is essential when comparing these SC machine topologies is the investment cost. For a long time the high cost has been one of the main challenges for SC machines to be competitive. In this paper we develop a method, employing 2D finite element (FE) computations, to optimize the machine topologies with respect to minimization of the active material cost. By using the method, we compare the three machine topologies and provide a guideline to the DDSCG designers to select a suitable machine topology. The first part of this paper describes the DDSCG and the three proposed machine topologies. The second part presents the method implementing FE methods to calculate the active material cost and electromagnetic (EM) torque and defines the objective function for optimization. The third part compares the three machine topologies in terms of active material cost, active material mass, synchronous reactance and phase resistance. In the end part the conclusions

are drawn.

2 Generator Description

The generator is of 10 MW, 9.65 rpm and 3.3 kV, and the used superconductor wire is MgB_2 at the temperature of around 20 K [17]. The generator is operated at its maximum torque point when the electromotive force is in phase with the corresponding phase current, or in other words the d-axis is 90 electrical degrees with respect to the axis of phase A just when phase A is carrying its amplitude current. The SC field winding is operated with a 25% safety margin to its in-field critical current density. The generator axial length is set such that the nominal torque is obtained when the armature bore diameter is fixed to 5 m. The constants of the generator are summarized in Table 1. The composite material for non-magnetic core structures is glass fiber (G10) at a cost of 15 €/kg which has a similar mechanical strength as steel but the mass density is only 1/4. The price of MgB_2 is set to its current market price of 4 €/m which may reduce significantly at a large scale deployment of MgB_2 based superconductor components. Copper and iron prices are 15 €/kg and 3 €/kg, respectively.

For this DDSCG, machine topologies T1, T2 and T3 are typically considered. They are distinguished in three core components: field yoke, armature tooth and armature yoke. In T1, only the armature yoke is made of iron while the other two core components are made of G10. In T2, both the field and armature yokes are made of iron while the armature teeth are made of G10. In T3, the three core components are all made of iron. The field pole core is made of G10 for all the three machine topologies.

The variables to be optimized are summarized in Table 2 and the geometrical variables are illustrated in Fig. 2. The effective air gap length of 40 mm is the distance from the armature bore to the outer field winding and includes the mechanical air gap length of 6 mm, the electromagnetic shield (i.e. the cryostat wall) thickness of 18 mm and the multi-layer insulation (MLI) thickness of 16 mm. The first constraint insures a positive width of the field coil sides and the second constraint limits the height of the armature teeth to be smaller than two times the height of armature yoke.

3 Method

With the genetic algorithm (GA) for optimization processing, the procedure of calculating the active material cost follows the flow diagram as illustrated in Fig. 3. When determining the operating current density and the EM torque per unit length, 2D FE methods are used, taking into account the non-linear B-J load curve of the field coil and the non-linear B-H magnetization curve of the magnetic iron.

3.1 Operating field current density

The operating current density of an SC winding must stay below the critical current density of the superconductor wires, otherwise the wires will leave their superconducting states. The critical current density as function of magnetic flux density and temperature is normally provided by the superconductor wire supplier. The machine topology determines the so-called load line which is defined as the maximum flux density of the SC coil with respect the current density flowing in the SC coil. The load line may be linear or not, depending on the saturation of iron core of the machine.

The load line crosses the critical characteristic as illustrated by the solid black line in Fig. 4. This intersection is on the boundary of the superconducting state which is insufficient for safe operation. A safety margin of 25% is therefore introduced for the current density (dashed line in Fig. 4).

The load line may, however, not be linear. So we cannot simply find one point on the load line and connect it to the origin linearly. It would also be too time consuming to find all the points on the load line by FE. Here a method is proposed to find the intersection by computing the maximum flux density of the SC field coil only a few times.

As illustrated in Fig. 5a, the unknown load line in red is not linear. The characteristic with 25% safety margin in blue crosses the load line at point X. This intersection is to be found. At first, we set a uniform current density, which is far higher than the needed, to the SC field winding. The computed maximum flux density in the SC field coil is at point A which must be located on the load line. We connect point A to the origin and this connecting line crosses the characteristic at point B. Secondly, as illustrated in Fig. 5b, we set the current density at point B uniformly to the SC field winding and compute the maximum flux density of the SC coil which must be at point C on the load line. We connect point C to the origin and this connecting line crosses the characteristic at point D. Then we repeat this process a few more times, as illustrated in Fig. 5c and the computed maximum flux density will finally get to point E which is close enough to point X within a preset tolerance , as illustrated in Fig. 5d and given by

$$B(k+1) - B(k) \leq \varepsilon, \quad k = 1, 2, 3, ... \tag{1}$$

where $B(k+1)$ is the maximum flux density of the field coil for the computation $k+1$ and $B(k)$ is the maximum flux density of the field coil for the previous computation k. Here the tolerance ε is 0.02 T. This final intersection point X is the operating point of the SC field winding, which is limited by the strongest flux density in the SC field coil. This search for intersection requires only 4 to 6 FE computations.

3.2 Electromagnetic torque

The EM torque obtained in 2D FE is the torque per unit length T_z. We have already defined the required nominal torque T_n, so the generator axial length

can be calculated by

$$l_s = T_n / T_z \tag{2}$$

We must take into account the torque ripples, otherwise the torque calculation would be incorrect. The torque ripples are caused by the armature winding distribution and the reluctance variation due to iron teeth. The average torque can be obtained by a two-step FE computation. In the first step, the d-axis of field winding is 90 electrical degrees with respect to the axis of phase A just when phase A is carrying its amplitude current, and the first torque T_h can be computed. In the second step, the armature winding is rotated by $1/2mpq$ of a mechanical cycle and accordingly the phase currents also vary in time by $1/2mq$ of the electrical cycle. The second torque T_l can then be computed in this position. The rotation of $1/2mpq$ is equal to an armature slot pitch, and by averaging T_h and T_l the average torque per unit length T_z is obtained. This method assumes that the torque ripples are not very large, otherwise the averaging should be done in a complete electrical cycle rather than with only two points. The result will show this assumption is satisfied since the torque ripples of the three topologies are up to 15% of the nominal torque.

3.3 Optimization objective function

The objective function of optimization is the active material cost given by

$$C_{act}(\mathbf{V}) = C_{SC} + C_{Cu} + C_{fy} + C_{fpc} + C_{at} + C_{ay} \tag{3}$$

where $\mathbf{V}$ is the variables to be optimized, C_{act}, C_{SC}, C_{Cu}, C_{fy}, C_{fpc}, C_{at} and C_{ay} are the costs of active materials, superconductor wires, field yoke, field pole cores, armature teeth and armature yoke, respectively. The cost is determined from the unit length usage of materials of the 2D FE model and multiplied by unit length costs. The length of the end winding of field and armature coils has been taken into account. The SC field coil is in the shape of racetrack and thus its end winding is modelled as semi-circles. The shape of the armature coil follows the conventional copper coil shape for a three-phase distributed winding.

This objective function is minimized by a generic algorithm NSGA-II ([18], [19]) which has been modified to this single-objective application. The optimization starts from a random set of variables and takes 40 individuals and 80 generations to converge [20].

3.4 Synchronous reactance

For the already optimized three machine topologies, FE methods are applied to calculate the synchronous reactance with the field current excitation. As the saturation of magnetic iron due to the field current excitation is very strong, FE computations are a simple way to solve this non-linear problem [21].

4 Comparison

The minimized active material cost of each topology and the corresponding active material mass are compared in Fig. 6. The resultant axial lengths of T1, T2 and T3 are 3.11 m, 2.41 m and 2.12 m, respectively. The optimized numbers of pole pairs are 11, 11 and 19, respectively. The optimal topology geometries and the corresponding magnetic fields are plotted in Fig. 7. Compared with the non-magnetic core, the use of iron core effectively reduces the active material cost with a limited influence on the mass. The synchronous reactance and the phase resistance shown in Fig. 8 imply that, by using more iron core components, the saturation gets more severe but the copper loss decreases.

The active material cost of T3 is the smallest and below 1 M€, and although T3 is 45% cheaper than T1, it is only 14% heavier, which are positive cost implications. T2 is not as cheap as T3 and its mass is the largest among the three topologies. T1 is the lightest with the highest cost. It can be observed that the copper takes up the majority of cost even with the high superconductor wire cost. The optimization process tries to minimize the use of expensive superconductor wires while to increase the use of less expensive copper and iron to achieve the same nominal torque. As indicated in Fig. 7 the SC field coil is very thin and flat, whereas the iron core and the copper area are large. Obviously, a reduced superconductor wire cost (as anticipated in case of a significantly increased MgB_2 superconductor market) could alter the design optimization, allowing for more superconductor material, while reducing the amount of copper, to minimize the overall active material cost.

The synchronous reactance does not go up when the topology turns from T1 to T3. The saturation due to the strong magnetic field excited by the SC field winding limits the increase of synchronous reactance. As illustrated in Fig. 7, the arrow flux lines show the saturation levels of the three optimized topologies. The resistance in per unit indicates the copper loss of the armature winding. From T1 to T3, some of the copper is replaced by iron to achieve the same torque, since iron is much cheaper, and the copper loss is consequently reduced.

5 Conclusion

A method has been developed to optimize a 10 MW DDSCG in terms of minimized active material cost. Calculation of the active material cost needs only 6 to 8 FE computations, which are acceptable for an optimization. By implementing this FE method to find the operating field current density and compute the average EM torque, three typical SC generator topologies have been optimized. Among the three topologies, the active material cost and mass, the synchronous reactance and the phase resistance are compared. The use of more iron core components, going from machine topologies T1 to T3, results in a lower active material cost with a limited increase of mass, a reduction of copper loss, and a small synchronous reactance due to heavy saturation.

Acknowledgment

This work is part of the INNWIND.EU project supported by the FP7 framework of EU, under grant agreement No. 308974.

References

[1] Li, H.; Chen, Z., "Overview of different wind generator systems and their comparisons," Renewable Power Generation, IET , vol.2, no.2, pp.123,138, June 2008, doi: 10.1049/iet-rpg:20070044.

[2] Semken, R.S.; Polikarpova, M.; Roytta, P.; Alexandrova, J.; Pyrhonen, J.; Nerg, J.; Mikkola, A; Backman, J., "Direct-drive permanent magnet generators for high-power wind turbines: benefits and limiting factors," Renewable Power Generation, IET , vol.6, no.1, pp.1,8, January 2012, doi: 10.1049/iet-rpg.2010.0191.

[3] Polinder, H.; Ferreira, J.A; Jensen, B.B.; Abrahamsen, AB.; Atallah, K.; McMahon, R.A, "Trends in Wind Turbine Generator Systems," Emerging and Selected Topics in Power Electronics, IEEE Journal of , vol.1, no.3, pp.174,185, Sept. 2013, doi: 10.1109/JESTPE.2013.2280428.

[4] Barnes, Paul N.; Sumption, Michael D.; Rhoads, Gregory L.; "Review of high power density superconducting generators: Present state and prospects for incorporating YBCO windings," Cryogenics, Volume 45, Issues 1011, OctoberNovember 2005, Pages 670-686, doi: 10.1016/j.cryogenics.2005.09.001.

[5] Abrahamsen, A. B. et al., "Superconducting wind turbine generators," Superconductor Science and Technology 23(3) 034019, 2010, doi:10.1088/0953-2048/23/3/034019.

[6] Klaus, G.; Wilke, M.; Frauenhofer, J.; Nick, W.; Neumuller, H.-W., "Design Challenges and Benefits of HTS Synchronous Machines," Power Engineering Society General Meeting, 2007. IEEE , vol., no., pp.1,8, 24-28 June 2007 doi: 10.1109/PES.2007.385756

[7] Terao, Y.; Sekino, M.; Ohsaki, H., "Electromagnetic Design of 10 MW Class Fully Superconducting Wind Turbine Generators," Applied Superconductivity, IEEE Transactions on , vol.22, no.3, pp.5201904,5201904, June 2012 doi: 10.1109/TASC.2011.2177628

[8] Jensen, B. B.; Mijatovic, N.; Abrahamsen, A. B., "Development of superconducting wind turbine generators," Journal of Renewable and Sustainable Energy, 5, 023137 (2013), doi: 10.1063/1.4801449.

[9] Carr, W.J. Jr., AC loss and macroscopic theory of superconductors. CRC Press, 2001.

[10] Magnusson, N.; Abrahamsen, A. B.; Liu, D.; Runde, M.; Polinder, H., "Hysteresis losses in MgB_2 superconductors exposed to combinations of low AC and high DC magnetic fields and transport currents," Physica C: Superconductivity, Available online 30 June 2014, doi: 10.1016/j.physc.2014.06.012.

[11] Kostopoulos, D., et al., "Feasibility Study of a 10 MW MgB_2 Fully Superconducting Generator for Offshore Wind Turbines," EWEA Offshore 2013, Frankfurt, Germany, 19-21 November 2013.

[12] 2014 [online] Available: http://www.innwind.eu.

[13] Fair, R. "Superconductivity for Large Scale Wind Turbines", DOE report DE-EE0005143, 2012.

[14] Ronghai Qu; Yingzhen Liu; Jin Wang, "Review of Superconducting Generator Topologies for Direct-Drive Wind Turbines," Applied Superconductivity, IEEE Transactions on , vol.23, no.3, pp.5201108,5201108, June 2013, doi: 10.1109/TASC.2013.2241387.

[15] Yingzhen Liu; Ronghai Qu; Jin Wang, "Comparative Analysis on Superconducting Direct-Drive Wind Generators With Iron Teeth and Air-Gap Winding," Applied Superconductivity, IEEE Transactions on , vol.24, no.3, pp.1,5, June 2014, doi: 10.1109/TASC.2013.2292309.

[16] Miller, T. J E; Hughes, A, "Comparative design and performance analysis of air-cored and iron-cored synchronous machines," Electrical Engineers, Proceedings of the Institution of , vol.124, no.2, pp.127,132, February 1977 doi: 10.1049/piee.1977.0022

[17] Abrahamsen, A. B. et al., "Design of an MgB_2 race track coil for a wind generator pole demonstration," J. Phys.: Conf. Ser. 507 032001, 2014, doi:10.1088/1742-6596/507/3/032001.

[18] Deb, K.; Pratap, A; Agarwal, S.; Meyarivan, T., "A fast and elitist multiobjective genetic algorithm: NSGA-II," Evolutionary Computation, IEEE Transactions on , vol.6, no.2, pp.182,197, Apr 2002, doi: 10.1109/4235.996017.

[19] 2014 [online]. Available: http://www.mathworks.nl/matlabcentral/fileexchange/31166-ngpm-a-nsga-ii-program-in-matlab-v1-4/content/nsga2.m.

[20] Bianchi, N.; Bolognani, S., "Design optimisation of electric motors by genetic algorithms," Electric Power Applications, IEE Proceedings - , vol.145, no.5, pp.475,483, Sep 1998, doi: 10.1049/ip-epa:19982166.

[21] Bianchi, N. Electrical Machine Analysis Using Finite Elements, CRC Press, 2005.

Table 1: Generator Parameters

Parameters	Value
Nominal torque	$T_n = 9.9$ MNm
Number of phases	$m = 3$
Number of slots per pole per phase	$q = 2$
Armature current density amplitude	$J_s = 3$ A/mm^2
Armature winding factor	$k_{fil} = 0.7$
Effective air gap length	$g_{eff} = 40$ mm
Armature bore radius	$r_s = 2.5$ m
Cryogenic temperature	20 K
MgB_2 price	4 €/m
G10 price	15 €/kg
Copper price	15 €/kg
Iron price	3 €/kg

Table 2: Variables and Constraints

Variable and constraint	Boundary
Number of pole pairs p	[2, 30]
Start angle of field coil α (elec. deg)	[10, 90]
End angle of field coil β (elec. deg)	[10, 90]
Height of field coil h_f	[10, 400]
Height of field armature slot h_s	[10, 400]
Tooth width/slot pitch b_t/τ_s	[0.2, 0.8]
Height of armature yoke h_{sy}	[10, 400]
Height of field yoke h_{ry}	[10, 400]
Linear constraint 1	$\alpha - \beta < 0$
Linear constraint 2	$0.5h_s - h_{sy} < 0$

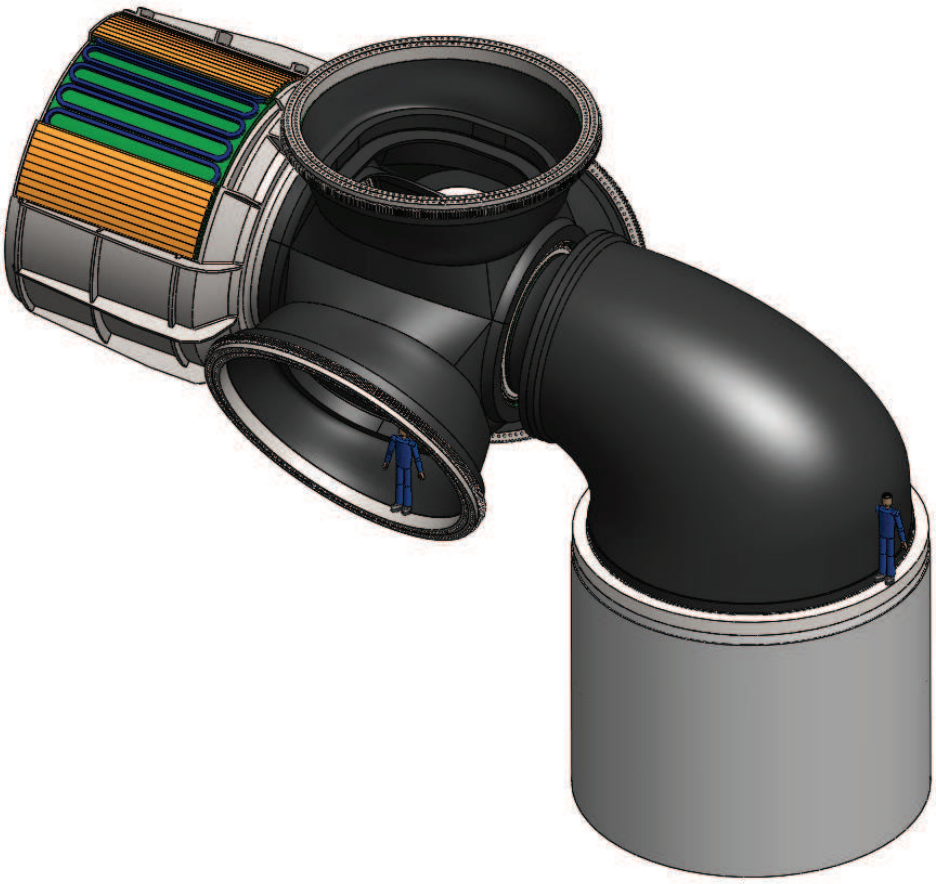

Figure 1: A DDSCG mounted onto the conceptual "king-pin" nacelle

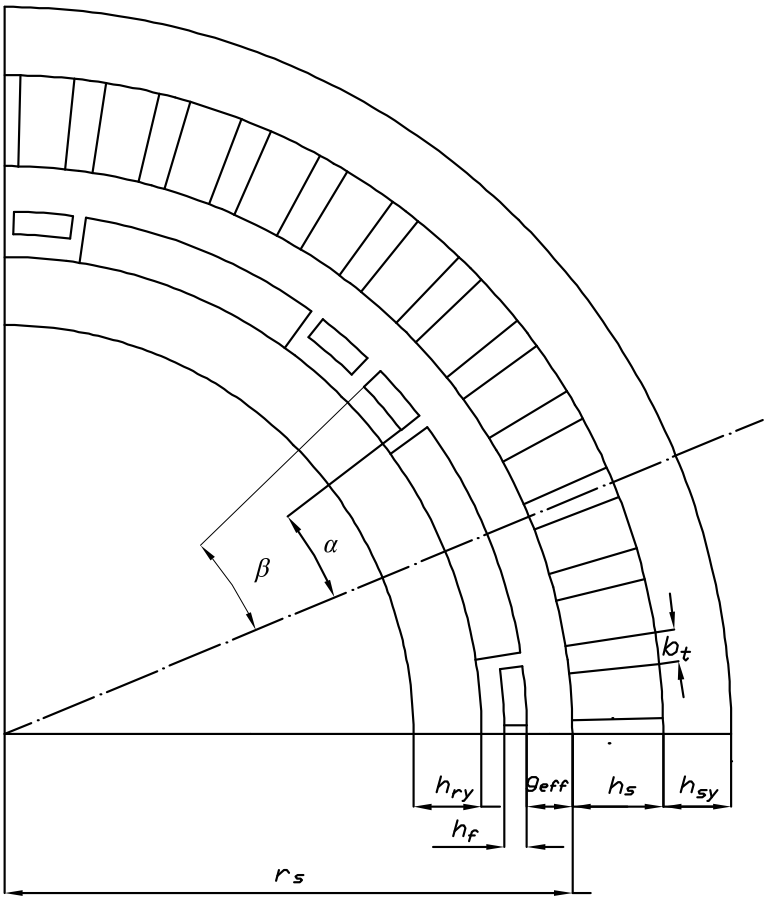

Figure 2: Geometrical variables and constants in a quarter of the generator cross section

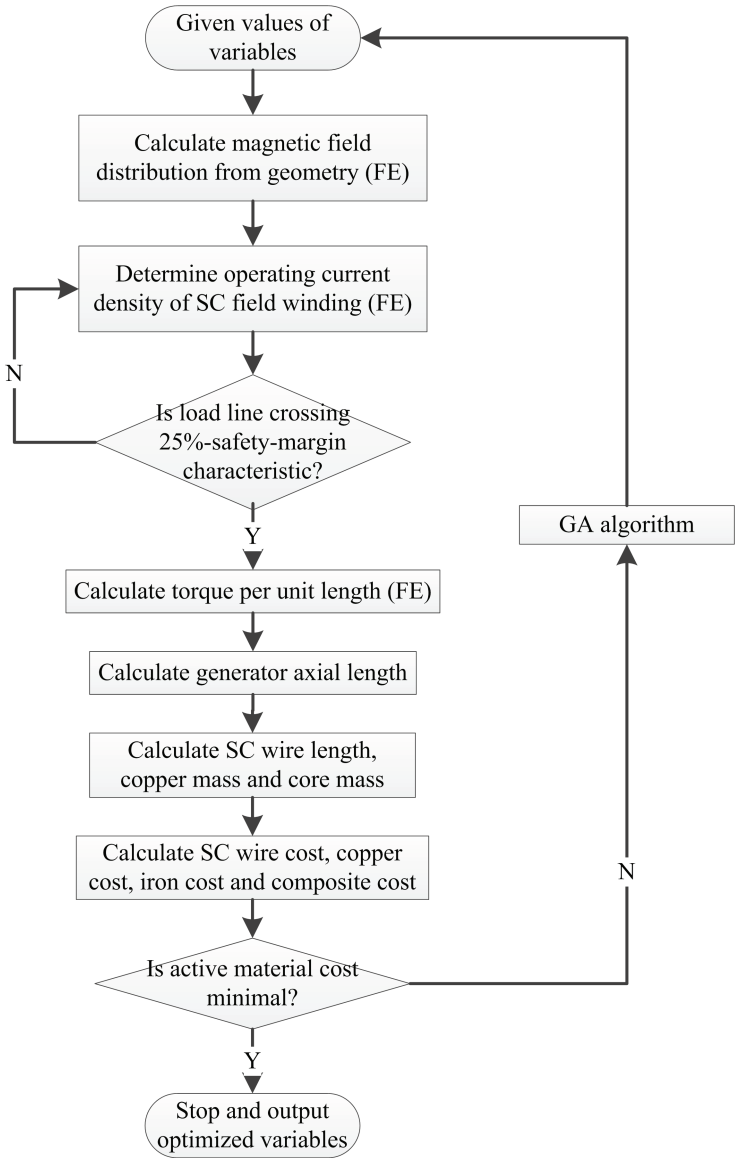

Figure 3: Flow diagram for calculating the active material cost and for implementing GA for optimization

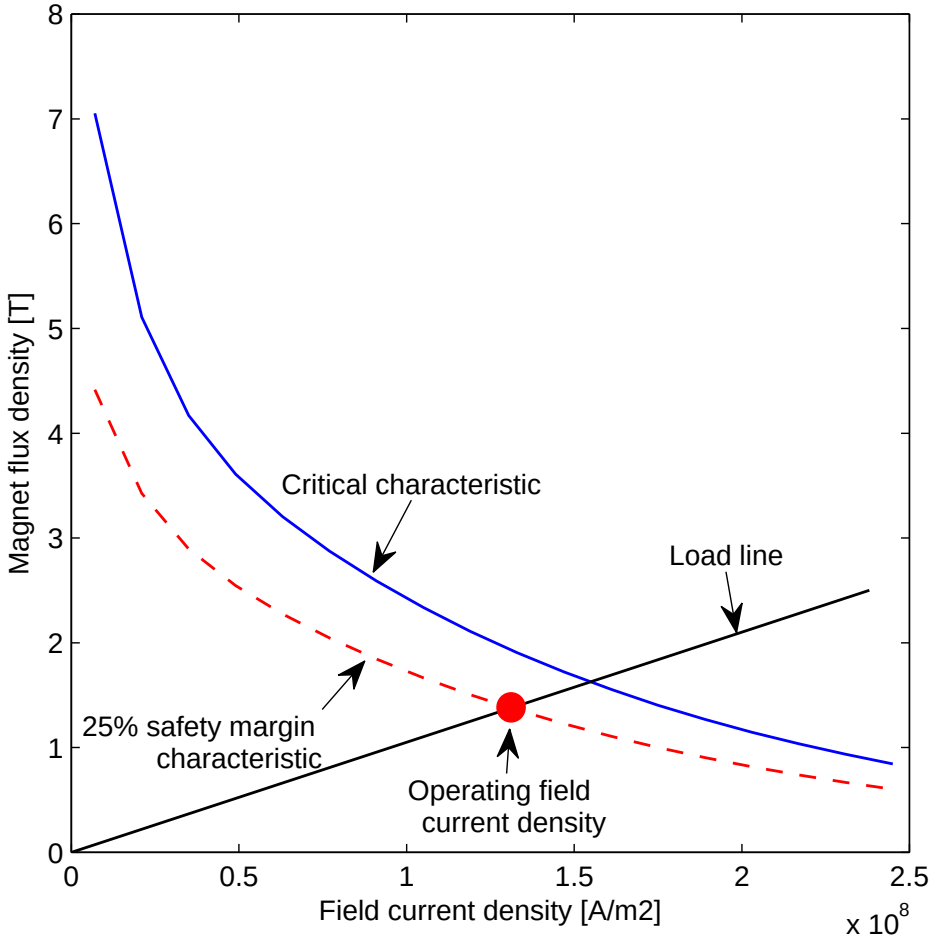

Figure 4: The definition of field winding operation point by crossing the load line and 25%-safety-margin characteristic at the temperature of 20 K

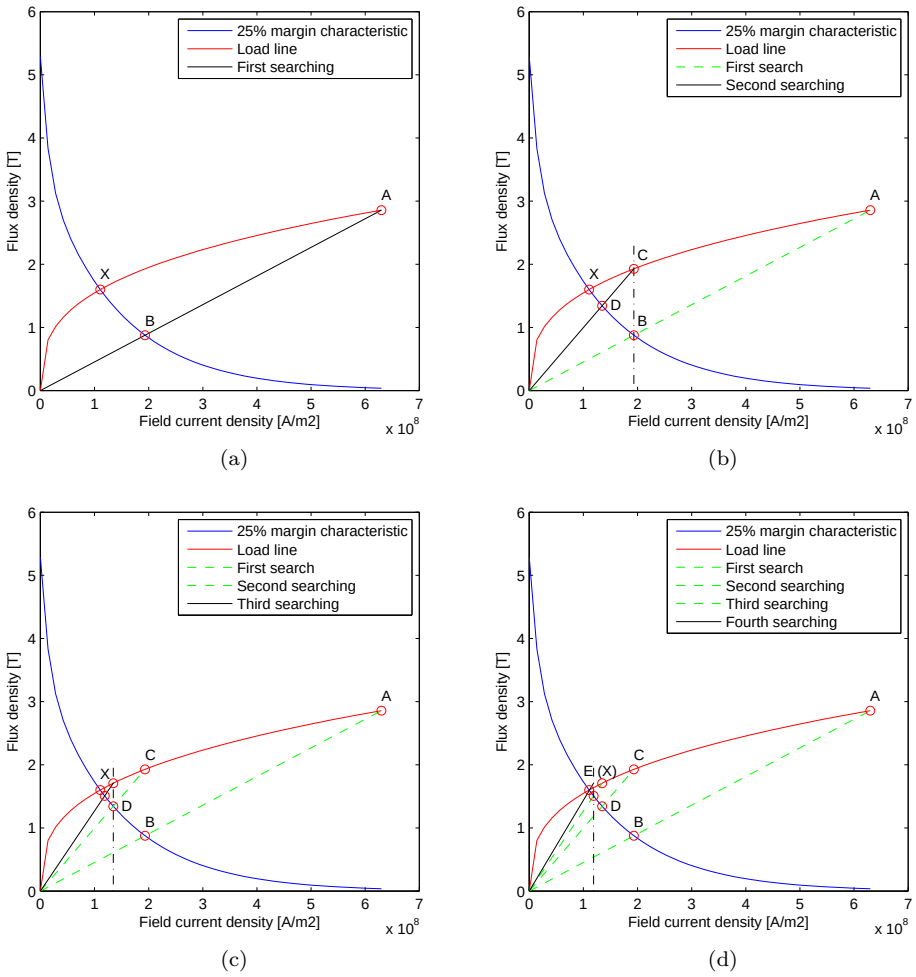

Figure 5: The illustration of finding the operating point with a non-linear load line by several steps of FE computation

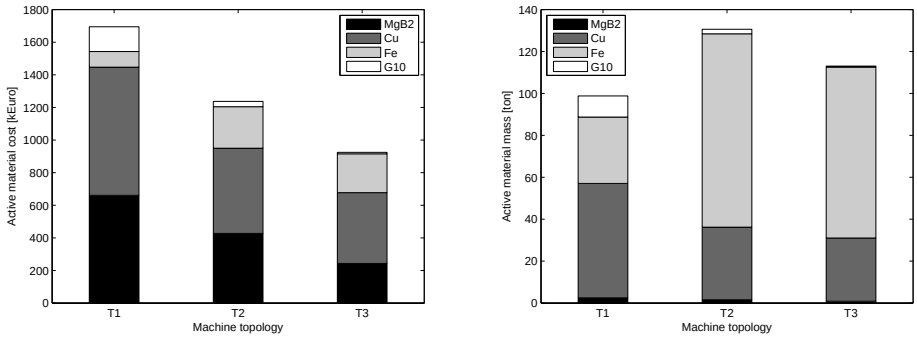

(a) Active material cost

(b) Active material mass

Figure 6: Active material cost and mass of compared machine topologies with a radius of 2.5 m and an active lengths of l_{T1} = 3.11 m, l_{T2} = 2.41 m and l_{T3} = 2.12 m. The optimal number of pole pairs are 11, 11 and 19 for T1 to T3 respectively.

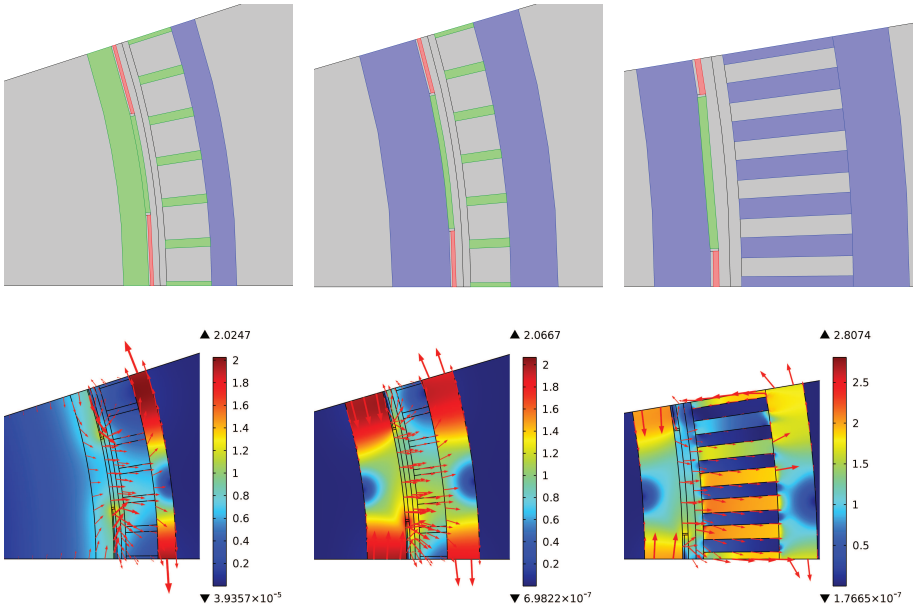

Figure 7: One pole of the optimized geometries and the corresponding magnetic flux densities of the three optimized machine topologies. From the left to the right are T1, T2 and T3. The colors of red, green and blue represent MgB_2, G10 and iron, respectively. The operating current densities of T1, T2 and T3 are 120.32 A/mm^2, 92.01 A/mm^2 and 102.61 A/mm^2, respectively. The maximum magnetic flux densities in the field coils of T1, T2 and T3 are 1.53 T, 1.85 T and 1.73 T, respectively

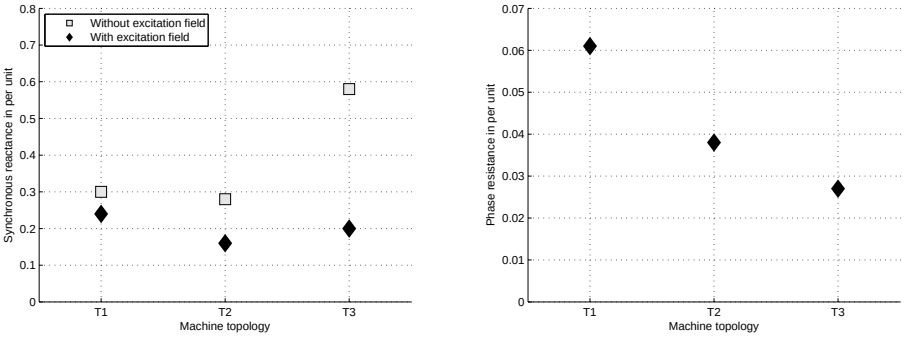

(a) Synchronous reactance (b) Phase resistance

Figure 8: Synchronous reactance and phase resistance